ISSN 0001-4370, Oceanology, 2024, Vol. 64, No. 3, pp. 446–461. © Pleiades Publishing, Inc., 2024.

MARINE GEOLOGY

Grain Size Properties of Surface Bottom Sediments from Chaun Bay

A. S. Ulyantsev[a, *], E. A. Streltsova[a], and A. N. Charkin[b, **]

[a] *Shirshov Institute of Oceanology, Russian Academy of Sciences, Moscow, Russia*

[b] *Il'ichev Pacific Oceanological Institute, Far Eastern Branch, Russian Academy of Sciences, Vladivostok, Russia*

**e-mail: uleg85@gmail.com*

***e-mail: charkin@poi.dvo.ru*

Received January 23, 2023; revised June 15, 2023; accepted July 18, 2023

Abstract—Based on the results of an analysis of 174 samples of bottom sediments collected at 48 stations in the Chaun Bay during the cruise 60 of the R/V *Akademik Oparin* (October 2020), it was found that their grain size distribution varies from poorly sorted silty clay to well sorted sand. The results of the study led to conclusion that the main sedimentation mechanisms in Chaun Bay are thermal abrasion, river runoff, and abrasion, as well as ice rafting and aeolian transport. The zoning of grain size types of bottom sediments is related to the bottom topography and consistent with areas affected by riverine runoff, abrasion, and thermal coastal abrasion, as well as with the direction of currents. The high occurrence of coarse clastic matter in sediments is evidence of abrasion of the coastal zone and active ice rafting of large (up to 15 cm) rock fragments. The vertical variability of the grain size parameters of the studied bottom sediments within the upper 20 cm layer reflects gradual Late Holocene intensification of terrigenous (fluvial and thermal abrasion) fluxes with the current effects of climate change in the Arctic.

Keywords: East Siberian Sea, bottom sediments, particle size, laser diffraction, particle size, sorting coefficients, correlation analysis

DOI: 10.1134/S0001437024700115

INTRODUCTION

The coastal zone of the Arctic shelf is a complex natural system, and in areas of its economic development, a natural–technogenic system, the functioning and evolution of which is governed by geological, geophysical, and geochemical processes. Potentially hazardous ones are degradation of the coastal zone under the impact of thermal abrasion and thermokarst, ice gouging of the bottom, subsoil degassing, and the inclusion of ancient organic matter contained in permafrost into the modern carbon cycle [2, 3, 15, 17–22, 24, 26]. Since for Russia the Arctic region is a zone of priority national interests, ensuring and strengthening economic and defense activity depends directly on its study. The need to forecast hazardous phenomena on the Arctic shelf is a very urgent problem. Interest in studying the morpholithodynamics of Chaun Bay is associated with poor knowledge of this water area and the small amount of field data. The increasing anthropogenic load is associated with commissioning of the Akademik Lomonosov floating nuclear power plant, based in the port of Pevek, into commercial operation in May 2020 [5]. In addition, the planned operation of the Northern Sea Route, one of the key transport and logistics hubs of which is the port of Pevek, focuses attention on the geological research of Chaun Bay.

The grain size characteristics of bottom sediments are an important tool in marine geology and lithology for characterizing sedimentation processes in various climatic conditions [6, 13, 23]. The degree of sorting of sedimentary material, the average diameter of particles, and their size distribution make it possible to judge the sedimentation conditions of the material, its genesis, and engineering-geological properties. Against the backdrop of increasing anthropogenic load, characterizing the grain size distribution of bottom sediments in the water area of Chaun Bay as an indicator of changes in the natural environment is an urgent problem, e.g., when forecasting anthropogenic risks and planning navigation. The aim of this study was to characterize the grain size distribution of the upper 20 cm layer of bottom sediments in Chaun Bay of the East Siberian Sea and analyze its spatial variability using a set of grain size indicators.

MATERIALS AND METHODS

The material for the study was 174 samples of bottom sediments collected at 48 stations on cruise 60 of the R/V *Akademik Oparin*, which took place from September 26 to November 11, 2020 [9]. An Ekman-type box sampler (0.25 m^2) was used for collecting material from the side of the vessel. Bottom sediments

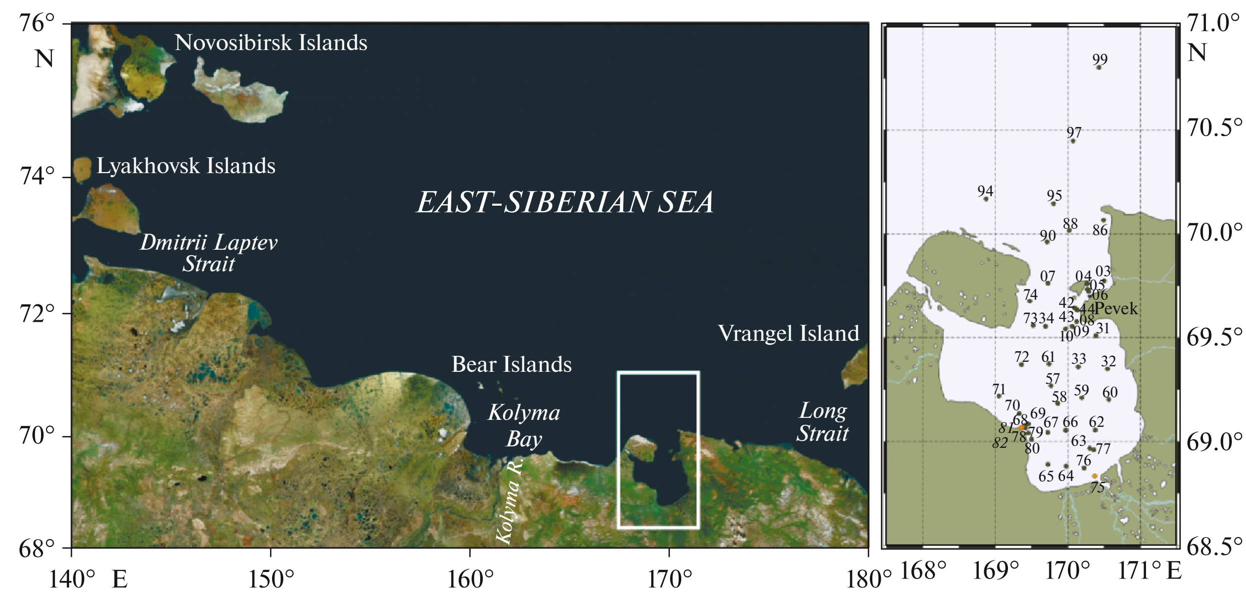

Fig. 1. Map of study area: right, diagram of location of bottom sediment sampling stations.

in shallow water (up to 10 m) were collected from a Chirok-320T motor launch. A Van Veen–type manual bottom grab (0.04 m^2) was used as a sampling tool. The location of stations and their coordinates are shown in Fig. 1 and Table 1, respectively. After an undisturbed sample of bottom sediments was raised on board the vessel, the bottom water was drained through an external hose, then insertions were made into the sediment sequence. Samples collected in shallow water were not stratified. Subsequent sampling, processing, and lithological description were carried out in the ship's laboratory. Samples (approximately 20 g of wet sediment) for grain size analysis were collected in plastic zip bags and stored in a refrigerator at 4°C until subsequent laboratory processing.

Grain size analysis of bottom sediments was carried out on the instrumentation base of the Shirshov Institute of Oceanology, Russian Academy of Sciences (IO RAS). For the analysis, we used the laser diffraction method after wet sieving of the sand fraction, which was done in order to eliminate the influence of large grains on the results of diffraction analysis [10, 25]. For sample preparation, a sample of sediment with natural moisture (2–3 g) was placed in a measuring glass, 20 mL of distilled water and 20 mL of 0.7% sodium hexametaphosphate solution were added, after which the sample was left for a day. The sand fraction was separated with a sieve with a hole diameter of 0.063 mm, and then into 0.063–0.125, 0.125–0.25, 0.25–0.5, 0.5–1, 1–2, and >2 mm fractions. The fractions separated in this way were dried to constant weight and weighed with an accuracy of 0.01 g.

Determination of the mass grain size distribution <63 μm was carried out on a SALD 2300 particle analyzer (Shimadzu, Japan) using a liquid dispersion module with constant stirring (1500 rpm) after ultrasonic exposure (power 40 W, frequency 32 kHz). The dispersant and background liquid consisted of distilled water. Immediately prior to diffraction analysis, the sample was immersed in an ultrasonic bath for 5 min and sonicated in the particle analyzer for 1 min immediately prior to analysis. Measurements were carried out using the WingSALD software package thrice for each sample. The results were averaged using R-script SALData, developed by D.G. Borisov (IO RAS). The study used binary logarithmic classification of sediments: >63 μm (sand), 10–63 μm (coarse silt), 2–10 μm (fine silt), and <2 μm (clay).

To characterize the grain size distribution of the studied sediments, the mass percentage distribution of fractions was calculated, as well as statistical parameters: mean particle diameter (M_Z), sorting coefficient (S_o), standard deviation (σ_I), skewness (Sk_I), and kurtosis (K_G) (Table 2). For statistical calculations, the percentiles p5, p16, p25, p50, p75, p84, and p95 were used, calculated for each sample by piecewise linear interpolation of cumulative size distributions. A previous study of the grain size distribution of sediments and permafrost from Buor-Khaya Bay, rich in sand-sized sedimentary material, showed underestimation of the results of calculating the M_z value by three percentiles [10]. Therefore, to calculate M_Z In this work, five percentiles were used: p5, p16, p50, p84, p95. Statistical processing of the results (correlation analysis) was performed using the Addinsoft XLSTAT Premium v2016.02 software package.

CHARACTERISTICS OF THE STUDY AREA

Chaun Bay is located in the southeastern East Siberian Sea and is a polygonal bay with a northwestern spatial orientation and many small rivers flowing

Table 1. Numbering, water depth, and coordinates of bottom sediment sampling stations

No.	Station	Water depth, m	Latitude, °N	Longitude, °E
1	03	14	69.772	170.503
2	04	11	69.759	170.266
3	05	21	69.732	170.274
4	06	22	69.720	170.288
5	07	25	69.761	169.728
6	08	14	69.578	170.122
7	09	15	69.553	170.062
8	10	16	69.541	169.972
9	31	12	69.509	170.390
10	32	11	69.349	170.549
11	33	16	69.358	170.146
12	34	20	69.554	169.695
13	42	17	69.640	170.098
14	43	19	69.637	170.112
15	44	18	69.632	170.132
16	57	16	69.267	169.772
17	58	15	69.182	169.864
18	59	16	69.209	170.195
19	60	12	69.201	170.569
20	61	18	69.372	169.744
21	62	13	69.053	170.380
22	63	13	68.967	170.302
23	64	11	68.879	169.978
24	65	10	68.888	169.728
25	66	15	69.052	169.974
26	67	14	69.043	169.726
27	68	12	69.075	169.419
28	69	12	69.082	169.460
29	70	11	69.134	169.335
30	71	10	69.218	169.051
31	72	10	69.369	169.362
32	73	12	69.558	169.523
33	74	11	69.676	169.480
34	75	6	68.832	170.372
35	76	10	68.871	170.228
36	77	11	68.958	170.358
37	78	11	69.064	169.420
38	79	10	69.040	169.459
39	80	9	69.008	169.502
40	81	5	69.069	169.382
41	82	2	69.065	169.359
42	86	22	70.064	170.497
43	88	16	70.017	170.020
44	90	14	69.961	169.714
45	94	18	70.168	168.878
46	95	20	70.145	169.807
47	97	29	70.447	170.076
48	99	30	70.800	170.432

Table 2. List of calculated grain size parameters

Parameter	Calculation formula	Reference
Mean diameter	$M_Z = \frac{p5 + p16 + p50 + p84 + p95}{5}$	[9]
Sorting coefficient	$S_o = \sqrt{\frac{p75}{p25}}$	[5]
Standard deviation	$\sigma_I = \frac{\phi84 - \phi16}{4} + \frac{\phi95 - \phi5}{6.6}$	[12]
Skewness	$Sk_I = \frac{\phi16 + \phi84 - 2\phi50}{2(\phi84 - \phi16)} + \frac{\phi5 + \phi95 - 2\phi50}{2(\phi95 - \phi5)}$	[12]
Kurtosis	$K_G = \frac{\phi95 - \phi5}{2.44(\phi75 - \phi25)}$	[12]

ϕ is the corresponding percentile of the grain size distribution of each sample, calculated according to [16].

into it [8], spanning an area of 9200 km^2, which is approximately 1% of the area of the East Siberian Sea [1]. The bay is distinguished by its relative isolation from open water, extends into the mainland for more than 100 km, and reaches a maximum width of 95 km, connecting with the East Siberian Sea through the Sredny and Maly Chaun and Pevek straits. From the east, the bay is bounded by steep Cape Shelagsky; in the western part, the inlet to the bay is blocked by Ayon Island, separated from the mainland by the narrow, shallow-water Maly Chaun Strait. From it towards the eastern coast and the islands of Maly and Bolshoy Routan lying near it, stretches the fairly wide Sredny Strait. Through it, during northeastern winds, cold water and ice from the open part of the East Siberian Sea enter the bay [12].

The polygonal tundra landscape is developed from the western (Ayon Island and Kyttyk Peninsula) and southern (mouth of the Chaun, Palyavaam, Puchevey, and Leluveem rivers) sides, where numerous thermokarst lakes, alases, and small rivers are concentrated. The western bank is low-lying, while the eastern bank is more elevated. The bottom topography shows alluvial fans, the largest of which are formed by the Chaun, Palyavaam, Ichvuveen, Leluvey, Mlelyyn, and Apapelgyn rivers, which flow into the southern, southeastern, and eastern parts of the bay. The average depth of the water area does not exceed 20 m; the maximum level (31 m) was recorded in the Pevek Strait (Fig. 2). According to [4], the composition of sedimentary material in Chaun Bay is largely determined by gravity flows of terrigenous material coming from land—thermal abrasion products of the coastal zone (Ayon Island) and river runoff.

The main current in Chaun Bay is the cyclonic circulation of waters entering through the western part of the bay and desalinated by river runoff [12]. In the head of the bay, under the influence of local river runoff, surface waters are desalinated to 14–16‰, warmed to + 7 to +8°C, and transformed into an estuarine-Arctic water mass [14]. Salinization to 23–25‰ as a result of convection on the surface and maintained warming up to +4 to +5°C, the newly transformed waters flow north into the East Siberian Sea along the eastern coast to Cape Shelagsky.

RESULTS

For most of the studied bottom sediments, stratification into oxidized, mixed, and reduced layers was noted. The oxidized layer, as a rule, is represented by fluid silty-clayey mud in the 0–2 cm range, from light brown to dark brown, often with a sand admixture. Below, usually in the 2–5 cm interval, is a mixed layer, represented by soft or fluid olive-colored silts, sometimes with a sand admixture. The mixed layer is underlain by reduced sediment strata, the color of which varies from light to dark gray. As a rule, these are viscous or viscoplastic silty clays. Common to the reduced sediment layers is the widespread distribution of hydrotroilite in the form of lenses, layers, and small black inclusions. Table 3 describes the sediments and calculated grain size parameters. As an example Fig. 3 shows the grain size distribution curves for bottom sediments of Chaun Bay with different lithological descriptions.

Coarse clastic (up to 15 cm) material was noted in the southwestern, southern, and central parts of Chaun Bay (stations 58, 59, 63, 67–70, 75, 76, 80), as well as in the Pevek Strait (stations 04–06), represented by fragments of shales, sandstones, siltstones, and granitoids. Pure and silty sands are concentrated in the western part (stations 69–74, 78–80). In the zone of influence of river runoff, concentrated in the south of the bay, sandy, silty–sandy, and silty varieties are common (stations 63–65, 75, 77). In the central and eastern parts (stations 31, 32, 57–62, 66), as well

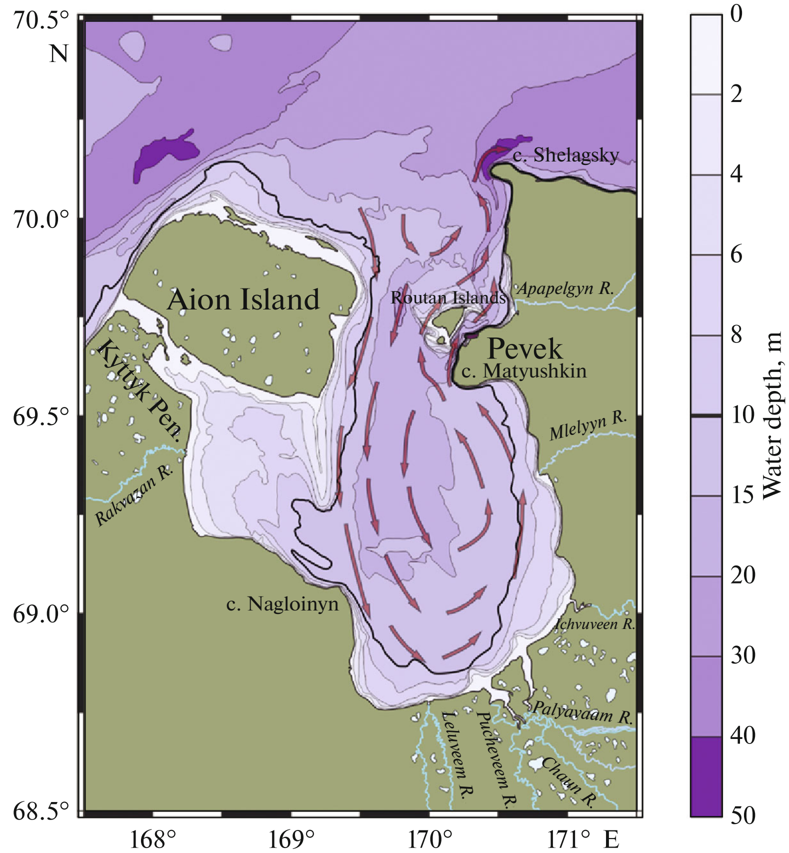

Fig. 2. Bathymetric map of Chaun Bay. Arrows indicate dominant direction of currents. Thick line, 10 m isobath.

as in the narrow inlet and at the outlet of the bay (stations 07, 86, 88, 90, 94, 95, 97, 99), sediments of the silty and silty–clayey fractions are common. Clayey sediments were noted at stations 33, 34, 61, and 86; in the surface layer at stations 97 and 99; and in the reduced layer at station 57.

The vertical cross-sectional variability of the grain size distribution of the studied sediments according to the calculated statistical parameters and the mass content of grain-size fractions within the upper 20 cm for the oxidized, mixed and reduced layers is insignificant (Tables 3, 4). The most significant difference is noted at stations 57, 67, 71, 72. For the studied bottom sediments, moving from the oxidized to the reduced layer, there is a general trend of a decrease in the average percentage contribution of sand fractions (>63 μm), associated with an increase in the contribution of silt and clay fractions (10–63, 2–10, and <2 μm), which is also accompanied by a gradual decrease in the average M_Z value (Table 4). At the same time, for the qualitative grain size characteristics of bottom sediments (S_o, σ_I, K_G, and Sk_I,) vertical variability along the studied section is extremely weak. We can only note the unexpressed trend of an increase with the depth of sediments in the average value of the sorting coefficient σ_I, which is explained by a general decrease in the contribution of sand fractions, characterized by a higher degree of sorting compared to fine-grained sediments.

In general, the calculated average values of the sorting coefficients (S_o and σ_I,) reflect the low degree of sorting of the studied sediments, the bulk of which are represented by silty–clayey and silty varieties. The average negative Sk_I values in combination with increased (>1) K_G values reflect a predominantly asymmetrical polymodal type of size distribution of the studied sediments characteristic of finer-grained varieties (Fig. 3). Therefore, a low degree of sorting is observed, reflected in increased S_o and σ_I values. For sediments of the sand fraction, in turn, the polymodality of the size distributions is weakly manifested, which is associated with a higher degree of sorting.

DISCUSSION

The results of the analysis of bottom sediments recovered from the bottom of Chaun Bay's water area revealed pronounced spatial variability of their grain size distribution depending on the distance from the coast, river runoff, and water depth. As an example in Fig. 4 shows the spatial distributions of the mass fraction (in %) of grain size fractions >63, 10–63, 2–10, and <2 μm in the oxidized layer of bottom sediments.

Table 3. Sampling horizons, lithological description, and grain size parameters of studied bottom sediments

Station	Horizon, cm	Description	M_Z, μm	S_o	σ_I	K_G	Sk_I
03	0–2	Silty mud, light brown with sand admixture, fluid	66.0	3.40	2.28	0.85	–0.31
	2–5	Silty mud, olive-colored with sand admixture, soft	50.0	3.35	2.16	0.80	–0.40
	5–10	Clayey mud, dark gray, viscoplastic, with hydrotroilite lenses	39.5	3.71	2.20	0.73	–0.32
	10–20	Same	38.2	3.26	2.14	0.80	–0.25
04	0–2	Clayey mud, light brown, fluid	10.3	2.11	1.70	1.07	0.03
	2–5	Clayey mud, olive-colored, soft	16.7	2.40	1.89	1.04	0.07
	5–10	Clay, dark gray, viscoplastic, with hydrotroilite lenses	9.8	1.99	1.56	1.09	–0.03
	10–20	Same	11.2	2.00	1.58	1.12	0.07
05	0–2	Silty mud, brown, with sand admixture, fluid	43.3	2.91	2.39	0.99	0.22
	2–5	Silty mud, olive-colored, soft	36.5	3.39	2.37	0.84	0.11
	5–10	Clayey mud, dark gray with hydrotroilite inclusions, viscoplastic	52.1	3.58	2.42	0.85	0.14
	10–20	Same	43.9	3.56	2.30	0.84	0.21
06	0–2	Silty–clayey mud with admixture of light Sand, brown, fluid	56.4	2.69	2.31	1.19	0.20
	2–5	Silty–clayey mud, olive-colored, soft	26.1	2.79	2.13	0.92	0.10
	5–10	Silty clay, gray, with traces of hydrotroilite, plastic	24.7	2.85	2.21	0.93	0.10
	10–20	Same	25.4	2.82	2.17	0.92	0.10
07	0–2	Silty–clayey mud, light brown, fluid	23.4	2.71	2.04	0.91	0.01
	2–5	Silty–clayey mud, olive-colored, soft	23.4	2.95	2.10	0.86	–0.05
	5–10	Silty–clayey mud, light gray, plastic	23.8	3.00	2.13	0.85	–0.05
	10–20	Same	23.6	2.97	2.12	0.85	–0.05
08	0–2	Silty–clayey mud, brown	28.5	2.69	2.01	0.90	–0.23
	2–5	Silty–clayey mud, olive-colored, denser	31.3	2.74	2.07	0.91	–0.27
	5–10	Silty clay, gray with large hydrotroilite inclusions, plastic	25.2	2.54	1.92	0.93	–0.24
	10–20	Same	28.3	2.65	2.00	0.92	–0.26
09	0–2	Silty–clayey mud, brown, fluid	22.0	2.35	1.83	1.00	–0.27
	2–5	Silty–clayey mud, olive-colored, soft	21.9	2.30	1.81	1.01	–0.30
	5–10	Silty clay, gray with isolated hydrotroilite inclusions, plastic	21.9	2.32	1.82	1.00	–0.28
	10–20	Same	21.9	2.31	1.81	1.01	–0.29
10	0–2	Silty–clayey mud, brown, fluid	19.3	2.33	1.83	1.04	–0.12
	2–5	Silty–clayey mud, olive-colored, plastic	18.5	2.31	1.78	1.01	–0.23
	5–10	Silty gray clay, viscoplastic	19.3	2.23	1.75	1.06	–0.11
	10–20	Same	18.9	2.27	1.77	1.03	–0.17
31	0–2	Silty–clayey mud, brown, fluid	22.1	2.40	1.80	0.96	–0.30
	2–5	Silty–clayey mud, olive-colored, soft	22.9	2.28	1.75	1.00	–0.29
	5–10	Silty clay, gray, plastic	20.5	2.24	1.74	1.02	–0.23
	10–20	Silty clay, dark gray, viscoplastic	25.1	1.78	1.54	1.31	–0.38

Table 3. (Contd.)

Station	Horizon, cm	Description	M_Z, µm	S_o	σ_I	K_G	Sk_I
32	0–2	Silty mud, dark brown, fluid	24.8	2.18	1.70	1.03	–0.29
	2–5	Clayey mud, gray, plastic	24.6	2.24	1.76	1.03	–0.29
	5–10	Clayey mud, dark gray, dense, hydrotroilite-enriched	21.1	2.34	1.81	1.00	–0.24
	10–20	Same	22.9	2.28	1.78	1.02	–0.27
33	0–2	Clayey mud, brown, fluid	128	2.26	1.72	0.99	–0.06
	2–5	Clayey mud, olive-colored, soft	19.3	2.27	1.85	1.12	0.02
	5–10	Clay, gray, plastic, with large hydrotroilite lenses	11.1	2.33	1.71	0.92	–0.10
	10–20	Clay, dark gray, viscoplastic, with large hydrotroilite lenses	13.0	2.15	1.66	1.03	–0.06
34	0–2	Clayey mud, brown, fluid	12.7	2.34	1.78	0.97	0.00
	2–5	Clayey mud, olive-colored, soft	18.1	2.61	1.96	0.96	0.02
	5–10	Clayey mud, dark olive, soft	12.7	2.54	1.83	0.89	–0.03
	10–20	Clayey mud, gray, soft, with hydrotroilite inclusions	16.0	2.56	1.92	0.94	0.04
42	0–2	Silty–clayey mud, brown, with sand admixture, fluid	39.4	2.77	2.28	1.09	0.19
	2–5	Silty–clayey mud, olive-colored, soft	29.3	2.94	2.20	0.94	0.12
	5–10	Silty clay, light gray, plastic	37.8	2.97	2.31	0.94	0.12
	10–20	Silty clay, gray, plastic	34.6	2.61	2.32	1.09	0.12
43	0–2	Silty–clayey mud, brown, with sand admixture, fluid	41.4	2.64	2.04	1.03	0.26
	2–5	Silty–clayey mud, olive-colored, with sand admixture, soft	40.2	2.49	2.09	1.10	–0.04
	5–10	Silty clay, gray, with sand admixture, plastic	49.6	2.73	2.31	1.09	–0.10
	10–20	Silty clay, dark gray, viscoplastic, with traces of hydrotroilite	38.0	2.88	2.29	1.03	0.11
44	0–2	Silty–clayey mud, brown, fluid	24.8	2.93	2.12	0.88	–0.02
	2–5	Silty–clayey mud, olive-colored, soft	25.5	2.90	2.10	0.88	–0.04
	5–10	Silty clay, dark gray, plastic, with massive layers of hydrotroilite	24.2	2.77	2.05	0.91	–0.01
	10–20	Same	20.6	2.72	2.00	0.92	0.00
57	0–2	Silty mud, light brown, fluid	59.4	2.64	2.34	1.26	0.20
	2–5	Silty–clayey mud, light gray, soft	18.0	2.45	1.94	1.03	0.06
	5–10	Clay, gray, plastic	13.7	2.31	1.88	1.06	0.07
	10–20	Clay, dark gray, with single hydrotroilite inclusions, plastic	8.2	2.17	1.65	0.98	–0.03
58	0–5	Silty mud, olive-colored, fluid	56.9	4.74	2.49	0.67	0.01
	5–10	Clayey mud, dark gray, plastic, with hydrotroilite inclusions	49.9	4.91	2.58	0.68	0.08
	10–20	Clayey mud, dark gray, dense, with thick accumulations of hydrotroilite	56.7	4.38	2.51	0.73	0.09
59	0–2	Silty–clayey mud, light brown, fluid	23.0	2.74	2.04	0.94	–0.06
	2–5	Silty–clayey mud, olive-colored, soft	22.4	2.57	1.96	0.97	–0.03
	5–10	Silty clay, gray, plastic	23.3	2.93	2.05	0.85	–0.13
	10–20	Silty clay, dark gray, plastic	13.8	2.61	1.87	0.88	–0.04

Table 3. (Contd.)

Station	Horizon, cm	Description	M_Z, μm	S_o	σ_I	K_G	Sk_I
60	0–2	Silty mud, brown, with sand admixture, fluid	29.2	2.09	1.68	1.06	–0.28
	2–5	Silty mud, olive-colored, soft	27.3	2.07	1.65	1.07	–0.30
	5–10	Clayey mud, dark gray, plastic	29.9	2.23	1.82	1.03	–0.30
	10–20	Clayey mud, dark gray, viscoplastic	29.3	2.17	1.78	1.06	–0.26
61	0–1	Clayey silt, light brown, fluid	9.5	2.02	1.58	1.06	–0.03
	1–5	Clayey mud, olive-colored, semifluid, with hydrotroilite inclusions	9.1	1.99	1.55	1.08	–0.05
	5–10	Clayey mud, gray, semifluid, with hydrotroilite inclusions	10.4	2.08	1.63	1.04	–0.06
	10–20	Clayey mud, gray, soft, with hydrotroilite inclusions	8.8	2.02	1.60	1.10	–0.01
62	0–2	Silty mud, dark brown, with sand admixture, fluid	30.2	2.30	1.78	0.96	–0.24
	2–5	Silty mud, olive-colored, with sand admixture, soft	30.5	2.38	1.85	0.96	–0.28
	5–10	Silty mud, gray, with sand admixture, soft	28.3	2.32	1.83	0.98	–0.27
	10–20	Clayey mud, dark gray, viscoplastic, with traces of hydrotroilite	43.2	1.86	1.63	1.33	–0.54
63	0–2	Sand, red-brown	252	1.33	0.80	1.57	–0.21
	2–5	Sand, light gray	215	1.56	1.33	1.50	–0.52
	5–10	Silty sand, gray, dense, with hydrotroilite inclusions	137	4.13	2.60	0.79	–0.34
	10–20	Silty sand, dark gray, dense, with hydrotroilite inclusions	102	4.22	2.79	0.80	–0.01
64	0–2	Sand, red-brown	87.3	1.18	0.49	1.75	–0.43
	2–10	Sand, olive-colored	81.0	1.20	0.86	3.30	–0.57
	10–20	Sand, light gray	84.1	1.19	0.62	2.25	–0.50
65	0–2	Sand, brown	79.8	1.28	0.60	1.23	–0.36
	2–10	Sand, olive-colored	79.3	1.26	0.58	1.33	–0.27
	10–20	Sand, light gray	79.6	1.27	0.59	1.28	–0.31
66	0–2	Silty–clayey mud, brown, with sand admixture, fluid	26.5	2.96	2.10	0.84	–0.07
	2–5	Silty–clayey mud, olive-colored, with sand admixture, soft	26.5	3.19	2.20	0.81	–0.04
	5–10	Silty clay, gray, soft, with hydrotroilite inclusions	28.3	3.38	2.17	0.75	–0.20
	10–20	Silty clay, dark gray, viscoplastic, with hydrotroilite inclusions	31.2	2.95	2.02	0.81	–0.39
67	0–2	Silty mud, brown, fluid	35.3	3.17	2.10	0.80	–0.37
	2–5	Olive-colored sandy–silty mud, soft	52.5	2.99	2.15	0.91	–0.37
	5–10	Silty sand, gray, dense	66.4	2.01	1.75	1.32	–0.38
	10–20	Same	69.7	1.94	1.94	1.47	–0.53
68	0–5	Sandy–silty mud, olive-colored, fluid	49.0	2.03	1.72	1.16	–0.50
	5–10	Sandy silt, gray, soft	59.4	1.94	1.77	1.34	–0.53
	10–20	Sandy silt, gray, dense	54.2	1.98	1.74	1.25	–0.51

Table 3. (Contd.)

Station	Horizon, cm	Description	M_Z, μm	S_o	σ_I	K_G	Sk_I
69	0–2	Silty sand, light brown	78.6	1.32	1.00	2.16	–0.38
	2–5	Silty sand, brown	91.7	1.34	1.13	2.44	–0.47
	5–10	Sandy silt, dark gray, soft, with hydrotroilite lenses	61.2	1.72	1.88	1.64	–0.62
	10–20	Sandy silt, dark gray, dense	67.8	1.64	1.35	1.50	–0.48
70	0–3	Sand, brown	122	1.60	1.43	1.69	–0.45
	3–10	Sand, olive-colored, with gray clay lenses	113	2.38	1.94	1.09	–0.51
	10–20	Sand, light gray, with gray clay lenses	118	1.87	1.63	1.37	–0.47
71	0–5	Silty sand, dark brown	78.3	1.42	1.08	1.70	–0.33
	5–10	Silty sand, dark gray, with hydrotroilite lenses	132	2.94	2.24	0.96	–0.28
	10–20	Same	105	2.02	1.59	1.11	–0.22
72	0–5	Sand, olive-colored	91.5	1.24	0.44	0.93	–0.02
	5–10	Gray silty sand	60.4	1.61	1.48	1.64	–0.60
	10–20	Clayey mud, dark gray, plastic, enriched with hydrotroilite	46.1	4.37	2.46	0.72	0.02
73	0–5	Silty sand, gray	104	1.79	1.90	1.65	–0.51
	5–10	Silty sand, gray	93.5	2.29	2.18	1.20	–0.51
	10–20	Silty sand, dark gray	99.0	1.98	2.01	1.43	–0.51
74	0–2	Silty sand, olive-colored	67.6	1.35	0.82	1.40	–0.35
	2–5	Silty sand, gray	59.1	1.60	1.41	1.64	–0.57
	5–10	Silty sand, dark gray	66.7	1.32	0.95	1.90	–0.41
	10–20	Same	62.9	1.44	1.13	1.71	–0.48
75	0–10	Silty sand, dark gray, with inclusions of plant residues	156	2.89	2.13	0.94	–0.24
76	0–3	Sand, red-brown	203	1.68	1.04	0.91	–0.28
	3–5	Silty sand, gray	184	2.09	1.91	1.32	–0.54
	5–10	Sand, dark gray, with hydrotroilite inclusions	164	2.16	1.98	1.28	–0.50
	10–20	Same	174	2.12	1.94	1.30	–0.52
77	0–2	Silty sand, red-brown	139	1.77	1.56	1.43	–0.06
	2–5	Silty sand, olive-colored	152	2.19	1.92	1.23	–0.24
	5–10	Silty sand, gray, plastic	123	2.78	2.43	1.08	–0.31
	10–20	Silty sand, dark gray, plastic, with hydrotroilite inclusions	125	3.15	2.49	0.97	–0.35
78	0–2	Sandy–silty mud, olive-colored, fluid	51.2	1.62	1.37	1.54	–0.48
	2–5	Sandy–silty mud, light gray, soft	52.8	1.49	1.07	1.48	–0.40
	5–10	Sandy silt, gray, plastic	51.8	1.53	1.22	1.62	–0.50
	10–20	Sandy silt, dark gray, viscoplastic	46.9	1.74	1.48	1.41	–0.45
79	0–2	Sandy–silty mud, olive-colored, fluid	53.0	1.48	1.14	1.59	–0.47
	2–5	Sandy–silty mud, light gray, soft	51.6	1.45	1.07	1.62	–0.45
	5–10	Sandy silt, gray, plastic	46.1	1.58	1.27	1.49	–0.47
	10–20	Sandy silt, dark gray, plastic, with hydrotroilite lenses	43.8	1.78	1.46	1.27	–0.47
80	0–2	Sandy–silty mud, olive-colored, fluid	64.0	1.41	0.88	1.33	–0.28
	2–5	Sandy-silty mud, light gray, soft	55.6	1.54	1.22	1.55	–0.48
	5–10	Sandy silt, gray, plastic	51.7	1.67	1.41	1.46	–0.50
	10–20	Sandy silt, dark gray, viscoplastic	53.6	1.60	1.31	1.50	–0.49

Table 3. (Contd.)

Station	Horizon, cm	Description	M_Z, µm	S_o	σ_I	K_G	Sk_I
81	0–10	Silty sand, gray	68.9	1.39	0.75	1.07	–0.23
82	0–10	Sand, dark gray	588	1.40	1.30	2.18	0.57
86	0–2	Silty–clayey mud, olive-colored, fluid	21.9	2.85	2.07	0.88	0.06
	2–5	Clayey mud, light gray, fluid	16.9	2.59	1.94	0.94	0.05
	5–10	Clayey mud, gray, soft	8.3	2.12	1.65	1.03	–0.05
	10–20	Clayey mud, dark gray, soft, with large lenses and hydrotroilite masses	20.3	2.67	1.96	0.91	0.00
88	0–2	Silty mud, olive-colored, fluid	39.6	3.13	2.08	0.81	–0.50
	2–5	Silty mud, light gray, fluid	48.5	1.90	1.81	1.34	–0.68
	5–10	Silty mud, gray, soft	34.7	3.20	2.07	0.78	–0.36
	10–20	Silty mud, gray, with traces of hydrotroilite	40.3	2.57	1.94	0.94	–0.53
90	0–2	Silty–clayey mud, olive-colored, with sand admixture, fluid	28.6	2.86	2.12	0.88	–0.14
	2–5	Silty mud, light gray, with sand admixture, soft	42.4	2.79	2.02	0.87	–0.51
	5–10	Clayey mud, gray, viscoplastic, with sand lenses	41.4	3.39	2.23	0.80	–0.30
	10–20	Clayey mud, gray, viscoplastic, with lenses of sand	57.6	1.98	1.81	1.29	–0.57
94	0–5	Silty–clayey mud, olive-colored, with sand admixture, fluid	31.3	3.51	2.20	0.75	–0.14
	5–10	Silty clay, dark gray, viscoplastic, with traces of hydrotroilite	28.9	3.50	2.25	0.76	–0.12
	10–20	Same	31.6	3.57	2.19	0.73	–0.29
95	0–2	Silty–clayey mud, olive-colored, with sand admixture, fluid	275	3.16	2.17	0.81	–0.17
	2–5	Silty–clayey mud, light gray, with sand admixture, fluid	31.4	3.05	2.18	0.85	–0.17
	5–10	Silty clay, gray, soft, with hydrotroilite inclusions	26.2	2.78	2.05	0.90	–0.26
	10–20	Silty clay, dark gray, viscoplastic, with hydrotroilite inclusions	33.5	3.53	2.32	0.79	–0.09
97	0–2	Clayey mud, olive-colored, fluid	9.4	2.11	1.67	1.05	–0.05
	2–5	Silty–clayey mud, light gray, with sand admixture, fluid	33.0	3.73	2.31	0.75	–0.04
	5–10	Silty–clayey mud, gray, with sand admixture, soft, with hydrotroilite lenses	27.1	3.16	2.24	0.84	0.01
	10–20	Silty clay, gray, plastic, with hydrotroilite lenses	24.5	2.94	2.15	0.90	0.04
99	0–2	Clayey mud, olive-colored, fluid	10.6	2.21	1.72	1.01	–0.04
	2–5	Silty–clayey mud, gray, fluid, with hydrotroilite inclusions	31.1	3.68	2.21	0.72	–0.14
	5–10	Silty clay, dark gray, plastic, with hydrotroilite lenses	30.0	3.43	2.24	0.77	–0.04
	10–20	Same	26.9	3.08	2.17	0.83	0.01

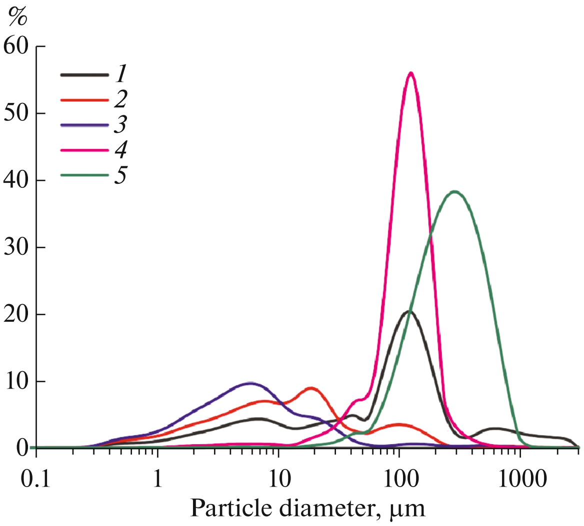

Fig. 3. Examples of grain size distributions in bottom sediments of Chaun Bay with different lithological descriptions. (*1*) station 03, 0–2 cm horizon (silty mud); (*2*) station 10, 0–2 cm horizon (silty–clayey mud); (*3*) station 61, 0–1 cm horizon (clayey mud); (*4*) station 74, 0–2 cm horizon (silty sand); (*5*) station 76, 0–3 cm horizon (sand).

In the southern and western parts of the studied water area, sand deposits are concentrated, characterized by an increased degree of sorting. The So value is characterized here by the smallest values, and its spatial distribution is visually consistent with the mass fraction of sand. The 10–63 μm fraction is concentrated mainly in the east, and increased concentrations (>50%) are noted in the southwest and western part of the narrow inlet to the bay. Fine-grained (2–10 and <2 μm) sediments are common in the central part, the mouth of the bay, and at the outlet to the East Siberian Sea.

The correlation and regression analysis results made it possible to assess the relationship between the studied grain size parameters and identify characteristic grain size associations of bottom sediments (Table 5). The noted strong positive correlation between the percentage content of the 2–10 and <2 μm fractions ($r = 0.97$) apparently indicates their related genesis in the studied sediments.

The same pair is characterized by a significant positive correlation with Sk_I, S_o, and σ_I and a negative correlation with M_Z, K_G, and >63 μm. In the first case, an increase in the proportion of fine-grained fractions in sediments leads to a decrease in the degree of sorting (So and σ_I increase), and size distributions, to a shift in the grain size distribution curve towards decreasing particle diameter (Sk_I also increases). In the second case, a general decrease in the contribution of fine-grained fractions leads to an increase in M_Z, and is also reflected in the size distributions, in which a more symmetrical grain size distribution curve is observed without pronounced secondary maxima (K_G tends to values <1). A significant negative correlation between the sand content (>63 μm) and 2–10 ($r = -0.83$) and <2 μm fractions ($r = -0.81$) is explained by the antagonism of the weight contribution of sand in sediments and differences in their lithological composition.

For the studied sediments, a negative relationship between the degree of sorting and asymmetry was noted (S_o-K_G and σ_I-K_G, $r = -0.75$ and -0.67, respectively) in combination with a positive correlation with the sand concentration (K_G->63 μm, $r = 0.62$). An increase in the mass fraction of the sand fraction in this case leads to polymodality of the grain size distribution curve (K_G increases), but at the same time the degree of sediment sorting increases (S_o and σ_I decrease). In the case of sediments of silty-pelitic and pelitic grain size, which make up the bulk of the analyzed samples, this pattern is violated due to the insignificant contribution of the >63 μm fraction. Direct correlation M_Z->63 μm ($r = 0.76$) along with negative ones from 10–63, 2–10 and <2 μm ($r = -0.47$, -0.58 and -0.56, respectively) indicates that the average particle diameter is largely determined by contribution of the sand fraction.

Based on the data obtained, a sketch map of the spatial distribution of grain size types of the surface (oxidized) layer of bottom sediments in the waters of Chaun Bay was compiled (Fig. 5). Sandy (mass fraction >63 μm no less than 70%) and silty–sandy (mass fraction >63 μm no less than 50%; 10–63 μm no less than 20%) sediments are common at depths of up to 15 m and concentrated in the western and southern parts of the bay. In the western, shallowest part of the bay, the grain size distribution of sediments is governed by the dynamics of thermal abrasion of polygonal–tundra permafrost deposits, which are widely developed here, and the latitudinal meridional distribution of sediments is associated with the influence of the current coming from the north. The input of sedimentary material through the Maly Chaun Strait, located between Ayon Island and the Kyttyk Peninsula, should not be excluded.

The southern part of Chaun Bay, in turn, is more susceptible to the influence of river runoff, which also transports a significant amount of thermal abrasion products. As in the western part of the bay, sediments of the sand and silty–sandy fractions are concentrated here, but the spatial distribution of the latter is significantly less. Apparently, this is due to greater particle sorting under the influence of hydrodynamics compared to thermal abrasion flows of sedimentary material concentrated in the west. There is also the influence of the prevailing current, which gradually decays to the south and cyclonically changes direction to the northeast and north. The area near Cape Nagloinyn, located between the western and southern parts of the bay, is distinguished by a relatively narrow zone of

Table 4. Ranges of values and average values of percentage contribution of grain size fractions and calculated parameters of studied bottom sediments in oxidized, mixed, and reduced layers

Parameter	Oxidized layer	Mixed layer	Reduced layer	Underlying reduced layer
*n**	48	45	45	36
>2 mm	0.00–11.3 / 0.44	0.00–1.80 / 0.06	0.00–2.96 / 0.17	0.00–1.87 / 0.05
1–2 mm	0.00–5.76 / 0.30	0.00–1.26 / 0.20	0.00–1.67 / 0.16	0.00–1.06 / 0.11
0.5–1 mm	0.00–2.14 / 0.49	0.01–1.92 / 0.40	0.00–1.96 / 0.34	0.00–1.69 / 0.26
250–500 μm	0.00–39.7 / 2.71	0.05–34.8 / 2.55	0.00–19.5 / 1.70	0.00–22.6 / 1.47
125–250 μm	0.01–44.3 / 6.56	0.08–37.2 / 5.64	0.06–36.0 / 4.93	0.07–30.1 / 3.25
63–125 μm	0.13–82.6 / 19.8	0.25–78.9 / 18.0	0.19–80.8 / 16.8	0.28–50.8 / 12.8
31–63 μm	3.05–41.2 / 15.0	3.23–44.7 / 15.5	2.40–41.5 / 14.9	1.64–35.9 / 16.3
10–31 μm	0.14–42.0 / 21.0	4.03–42.8 / 22.8	3.36–42.5 / 23.6	9.03–46.7 / 25.6
2–10 μm	0.00–50.3 / 23.0	2.04–50.9 / 23.4	1.02–50.57 / 24.9	7.15–50.7 / 26.7
<2 μm	0.00–24.4 / 10.7	0.45–21.4 / 11.5	0.41–27.32 / 12.5	3.31–27.7 / 13.4
M_Z, μm	9.4–588 / 67.1	9.1–215 / 52.3	8.33–164 / 47.5	8.24–174 / 40.7
S_o	1.18–4.74 / 2.28	1.20–4.91 / 2.46	1.19–4.38 / 2.56	1.44–4.22 / 2.47
σ_I	0.44–2.49 / 1.67	0.58–2.58 / 1.84	0.59–2.60 / 1.88	1.13–2.79 / 1.89
K_G	0.67–2.18 / 1.14	0.68–3.30 / 1.15	0.72–2.25 / 1.08	0.79–1.71 / 1.07
Sk_I	–0.51... +0.57 / –0.16	–0.68... +0.12 / –0.24	–0.62... +0.14 / –0.22	–0.57... +0.21 / –0.20

* Number of samples.

coarse-grained sediment distribution, caused by the relative isolation of the southwestern part of Chaun Bay from the influence of river runoff and thermal abrasion, and the basis of the petrofund of bottom sediments here is shales, partially emerging on the land surface in the form of slabs near Cape Nagloynyn [12].

Sediments of the silt fraction (mass content of the 10–63 μm fraction is no less than 50%; of the 2–10 μm fraction, no less than 20%) are concentrated in the southwestern and eastern parts of Chaun Bay in the depth range of 15–20 m. The area of their spatial distribution is adjacent to the zone of silty–sandy sediments, gradually turning into silty. As in the case of coarse-grained varieties, the distribution of sediments of the silt fraction is associated with the dynamics of river runoff, thermal abrasion, and currents, and the observed spatial fluctuations are apparently associated with the influence of seasonal ice discharge and aeolian transport of sedimentary material.

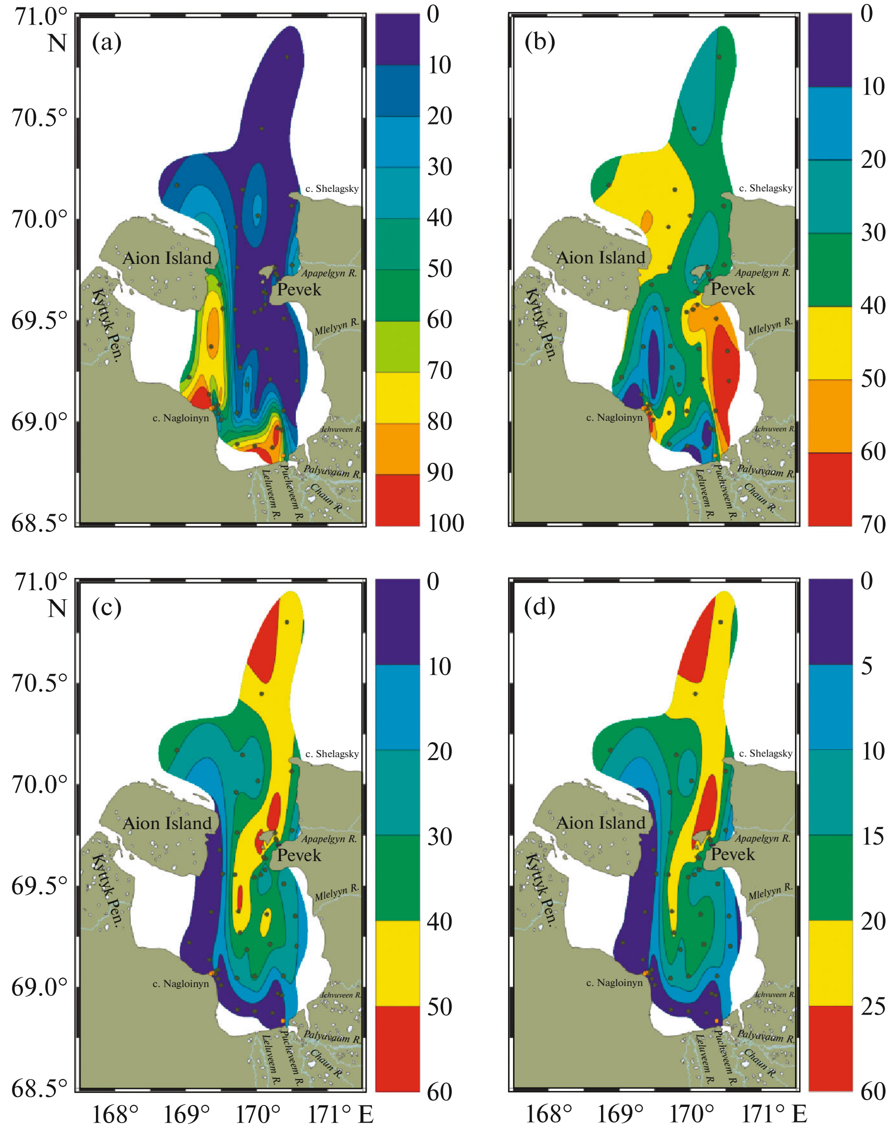

Fig. 4. Maps of spatial distribution of mass fraction (in %) of grain size fractions in surface (oxidized) layer of sediments. (a) >63 μm fraction; (b) 10–63 μm fraction; (c) 2–10 μm fraction; (d) <2 μm fraction.

Table 5. Correlation matrix of grain size parameters of studied sediments (n = 174). Values of the Pearson correlation coefficient r >0.5 and <–0.5 are highlighted in bold; r values close to 0.5 and –0.5 are in italics

Parameter	M_Z	S_o	σ_I	K_G	Sk_I	>63 μm	10–63 μm	2–10 μm	<2 μm
M_Z	–	–0.229	–0.222	0.418	–0.075	**0.756**	*–0.474*	**–0.583**	**–0.564**
So	–0.229	–	**0.883**	**–0.745**	0.423	–0.412	–0.011	*0.470*	**0.530**
σ_I	–0.222	**0.883**	–	**–0.665**	0.392	*–0.493*	0.044	**0.534**	**0.579**
K_G	0.418	**–0.745**	**–0.665**	–	–0.422	**0.615**	–0.223	**–0.566**	**–0.593**
Sk_I	–0.075	0.423	0.392	–0.422	–	–0.444	–0.280	**0.710**	**0.693**
>63 μm	**0.756**	–0.412	*–0.493*	**0.615**	–0.444	–	**–0.534**	**–0.834**	**–0.805**
10–63 μm	*–0.474*	–0.011	0.044	–0.223	–0.280	**–0.534**	–	–0.016	–0.054
2–10 μm	**–0.583**	*0.470*	**0.534**	**–0.566**	**0.710**	**–0.834**	–0.016	–	**0.971**
<2 μm	**–0.564**	**0.530**	**0.579**	**–0.593**	**0.693**	**–0.805**	–0.054	**0.971**	–

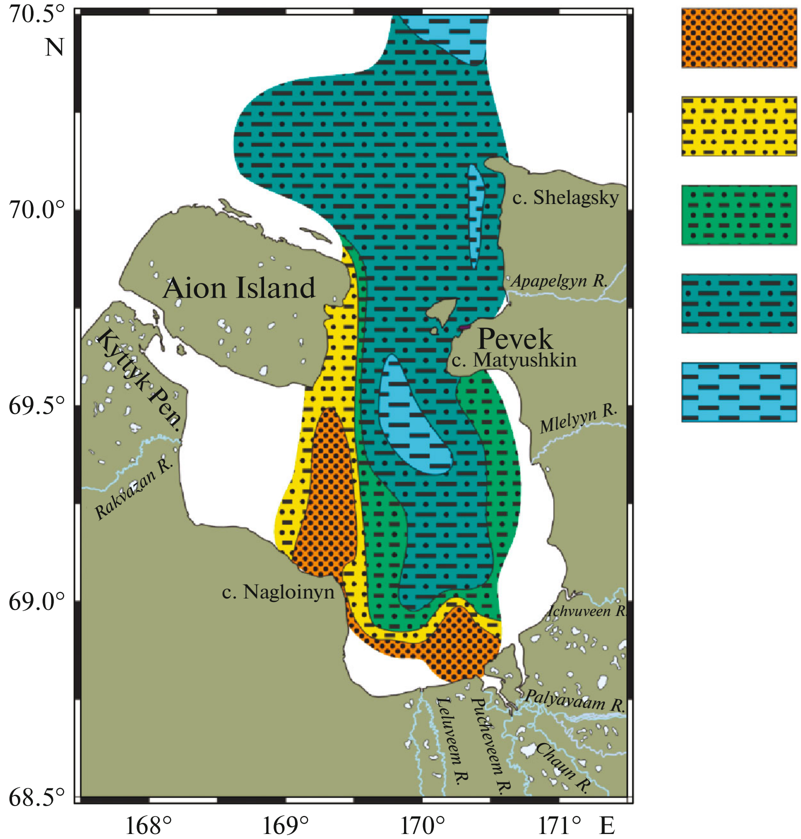

Fig. 5. Map of spatial distribution of granulometric types of bottom sediments of surface (oxidized) layer. (*1*) Sediments of sand fraction; (*2*) sediments of silty–sandy fraction; (*3*) sediments of silt fraction; (*4*) sediments of silty–clayey fraction; (*5*) sediments of clay fraction.

In the central part of Chaun Bay, in the narrow inlet, and at the outlet to the East Siberian Sea, in the depth range of 15–30 m, silty–clayey sediments are common (the mass content of the 10–63 μm fraction is no less than 20%; of the 2–10 and <2 μm fractions, no less than 50%) and pelitic (the mass content of the 2–10 μm fraction is no less than 50%; of the <2 μm fraction, no less than 20%). The latter are distributed in compact zones in the central part of the bay, along the eastern part of the narrow inlet, and in the north. This zoning is associated with isolation from the influence of river runoff and thermal abrasion and is associated with currents that favor hydrodynamic sorting of the finest-grained fractions. The main area of the central part and narrow inlet of the studied water area is occupied by sediments of the silty–clayey fraction. They are characterized by a relatively low degree of sorting, associated with a wide range of size groups in the grain size distribution spectra. The zoning of the distribution of this group of sediments is also associated with the distance from the influence of river runoff, abrasion, and thermal abrasion, and the variability of the grain size distribution is facilitated by the dynamics of currents, seasonality of freeze-up, and wind distribution of particles. The influence of seasonal surge winds, which contribute to the spatial redistribution of bottom sediments at the seabed, should not be excluded.

CONCLUSIONS

The set of data obtained as a result of the study on the grain size distribution of seabed surface sediments of Chaun Bay of the East Siberian Sea made it possible to characterize its spatial variability, the formation of which was primarily influenced by regional physical and geographical factors, lithodynamics, and the genesis of sedimentary material. The zoning of granulometric types of sediments revealed here is associated with the bottom topography and is consistent with the areas of influence of river flow, thermal abrasion, abrasion, and direction of currents. The recorded trend of a decrease in the mass fraction of sand during the transition from the oxidized to the reduced layer, accompanied by a mutual increase in the contribution of finer-grained fractions and a decrease in the average particle diameter, indicates activation in modern conditions of terrigenous (river and thermal abrasion) fluxes carrying large quantities of sandy material.

The results obtained in this study agree with previously obtained data [4] and confirm the currently observed trends in the variability of the natural environment of the Arctic, most often associated with climate fluctuations [18, 20–22, 24]. Taking into account the insignificant bioproductivity of Chaun Bay's water area [11, 12], analysis of the calculated grain size parameters allows us to conclude that the studied sediments are characterized by pronounced polymictity and detrital origin. The variability of the grain size characteristics in the oxidized, mixed, and reduced layers of bottom sediments established as a result of the study reflects the variability of the physical and geographical conditions of the morpholithogenesis of Chaun Bay at individual time stages of sedimentation within the upper 20 cm layer of sediments. Ultimately, this variability largely determined the grain size composition of the studied sediments. At the same time, the influence of river runoff, thermal abrasion, abrasion, as well as ice- and aeolian-related sedimentation, have remained decisive.

ACKNOWLEDGMENTS

The team of authors expresses gratitude to P.Yu. Semkin and V.L. Semin for their assistance in recovering bottom sediments in shallow coastal conditions.

FUNDING

Analytical work and interpretation of the results were supported by the Russian Science Foundation (project no. 19-77-10044). Expeditionary work was supported by state assignments (topic nos. FMWE-2021-0005 and FWMM-2019-0005).

ETHICS APPROVAL AND CONSENT TO PARTICIPATE

This work does not contain any studies involving human and animal subjects.

CONFLICT OF INTEREST

The authors of this work declare that they have no conflicts of interest.

REFERENCES

1. I. S. Zonn, A. G. Kostyanoi, and A. V. Semenov, *East Siberian Sea: Encyclopedia* (Mezhdunar. otnosheniya, Moscow, 2014) [in Russian].
2. O. V. Dudarev, A. N. Charkin, N. E. Shakhova, et al., *Present Lithomorphogenesis on the Eastern Arctic Shelf of Russia* (Izd. Tomsk. Politekh. Univ., Tomsk, 2016) [in Russian].
3. S. L. Nikiforov, L. I. Lobkovskii, N. N. Dmitrevskii, et al., “Expected geological and geomorphological risks along the Northern Sea Route,” Dokl. Earth Sci. **466**, 75–77 (2016).
4. N. A. Poltavskaya, E. V. Gershelis, I. A. Oberemok, et al., “Features of the composition of organic matter in bottom sediments of Chaun Bay (East Siberian Sea),” Izv. Tomsk. Politekh. Univ. Inzh. Georesur. **334** (2), 130–146 (2023).
5. TASS. Russia has put into commercial operation the world's first floating nuclear power plant. https://tass.ru/ekonomika/8540307. Accessed January 22, 2023.
6. V. N. Sval'nov and T. N. Alekseeva, *Granulometric Composition of Sediments of the World Ocean* (Nauka, Moscow, 2005) [in Russian].
7. *The System of the Laptev Sea and Adjacent Arctic Seas: Current State and History of Development*, Ed. by Kh. Kassens (Izd. Mos. Gos. Univ., Moscow, 2009) [in Russian].
8. A. Ya. Stremyakov, “On the question of the origin of oriented lakes,” in *Permafrost Rocks of Various Regions of the USSR* (Izd. Akad. Nauk SSSR, Moscow, 1963), pp. 75–107.
9. A. S. Ulyantsev, A. N. Charkin, V. L. Syomin, et al., “Geological studies of the upper sedimentary strata of Chaun Bay during cruise 60 of the R/V *Akademik Oparin*,” Oceanology **61** (4), 584–585 (2021).
10. A. S. Ulyantsev, S. Yu. Bratskaya, and Yu. O. Privar, “Grain size properties of the bottom sediments from Buor-Khaya Bay,” Oceanology **60** (3), 393–404 (2020).
11. “Ecosystems and fauna of the Chaun Bay and adjacent waters of the East Siberian Sea,” in *Studies of Sea Fauna*, Ed. by A. O. Skarlato (Zool. Inst., St. Petersburg, 1994), Vol. 48 (56) [in Russian].
12. “Ecosystems, flora, and fauna of the Chaun Bay and adjacent waters of the East Siberian Sea,” in *Studies of Sea Fauna*, Ed. by A. O. Skarlato (Zool. Inst., St. Petersburg, 1994), Vol. 47 (55) [in Russian].
13. R. L. Folk and W. C. Ward, “Brazos river bar: A study in the significance of grain size parameters,” J. Sediment. Petrol. **27**, 3–26 (1957).
14. A. N. Golikov and V. G. Averincev, “Distribution patterns of benthic and ice biocoenoses in the high latitudes of the polar basin and their part in the biological structure of the world ocean,” in Polar Oceans (Arctic Inst. of North America, Canada, 1977), pp. 331–360.
15. F. Günther, P. P. Overduin, I. A. Yakshina, et al., “Observing Muostakh disappear: Permafrost thaw subsidence and erosion of a ground-ice-rich island in response to Arctic summer warming and sea ice reduction,” The Cryosphere **9**, 151–178 (2015).
16. W. C. Krumbein, Size frequency distributions of sediments,” J. Sediment. Petrol. **4**, 65–77 (1934).
17. H. Lantuit, D. Atkinson, P. P. Overduin, et al., “Coastal erosion dynamics on the permafrost-dominated Bykovsky Peninsula, North Siberia, 1951–2006,” Polar Res. **30**, 7341 (2011).
18. J. Martens, B. Wild, F. Muschitiello, et al., “Remobilization of dormant carbon from Siberian-Arctic permafrost during three past warming events,” Sci. Adv. **6** (42) (2020).
19. L. Schirrmeister, G. Grosse, G. Schwamborn, et al., “Late Quaternary history of the accumulation plain north of the Chekanovsky Ridge (Lena Delta, Russia): A multidisciplinary approach,” Polar Geogr. **27** (4), 277–319 (2003).

20. E. A. G. Schuur, A. D. McGuire, C. Schädel, et al., "Climate change and the permafrost carbon feedback," Nature **520**, 171–179 (2015).
21. Semiletov, I. Pipko, Ö. Gustafsson, et al., "Acidification of East Siberian Arctic Shelf waters through addition of freshwater and terrestrial carbon," Nat. Geosci. **9**, 361–365 (2016).
22. N. Shakhova, I. Semiletov, and E. Chuvilin, "Understanding the permafrost-hydrate system and associated methane releases in the East Siberian Arctic Shelf," Geosciences **9** (6), 251 (2019).
23. J. Strauss, L. Schirrmeister, S. Wetterich, et al., "Grain-size properties and organic-carbon stock of Yedoma Ice Complex permafrost from the Kolyma lowland, northeastern Siberia," Global Biogeochem. Cycl. **26**, GB3003 (2012).
24. M. R. Turetsky, B. W. Abbott, M. C. Jones, et al., "Permafrost collapse is accelerating carbon release," Nature **569**, 32–34 (2019).
25. S. Ulyantsev, E. A. Streltsova, and A. N. Charkin, "Lithological and granulometric data for the upper sedimentary layer of the Chaun Bay, East Siberian Sea," Data in Brief **46**, 108813 (2023).
26. B. Wild, N. Shakhova, O. Dudarev, et al., "Organic matter composition and greenhouse gas production of thawing subsea permafrost in the Laptev Sea," Nat. Commun. **13**, 5057 (2022).